Modeling of channel patterns in short tidal basins

Raffaele Marciano,[1] Zheng Bing Wang,[2] Anneke Hibma, and Huib J. de Vriend[2]
Delft University of Technology, Delft, The Netherlands

Andrea Defina
Dipartimento Ingegneria Idraulica Marittima Ambientale e Geotecnica, Universitá di Padova, Padova, Italy

Received 10 September 2003; revised 5 October 2004; accepted 12 October 2004; published 7 January 2005.

[1] We model branching channel patterns in short tidal basins with two methods. A theoretical stability analysis leads to a relationship between the number of channels and physical parameters of the tidal system. The analysis reveals that width and spacing of the channels should decrease as the slope of the bottom profile and the Shields parameter increase and as the mean water depth decreases. In general, the channel depth should halve at every bifurcation. These theoretical results agree well with the field data from the Dutch Wadden Sea. A numerical model based on Delft3D, a software system of WL/Delft Hydraulics, is used to simulate the time evolution of a channel network in a geometrically simplified basin of similar dimensions as the Wadden Sea basins. The resulting channel network displays a three-times branching behavior, similar to the three- to four-times branching patterns observed in the Wadden Sea. The simulated channel pattern satisfies the relation derived from the theoretical analysis. The results of this pattern analysis provide for additional validation of two-dimensional/three-dimensional process-based morphodynamic models of tidal basins.

Citation: Marciano, R., Z. B. Wang, A. Hibma, H. J. de Vriend, and A. Defina (2005), Modeling of channel patterns in short tidal basins, *J. Geophys. Res.*, *110*, F01001, doi:10.1029/2003JF000092.

1. Introduction

[2] Tidal embayments are found in many coastal areas all around the world. A significant part of the world's coastline is formed by barrier island coasts, and many other tidal coasts are interrupted by estuaries and lagoon inlets. These tidally forced systems are important from an ecological, economical and recreational point of view. Besides, they have a considerable impact on the shorelines that they interrupt, through their influence on the sediment budget [*Stive and Wang*, 2003]. Therefore it is important to understand and predict the morphodynamic behavior of these complex systems.

[3] The geometric characteristics are strongly influenced by the tidal and wind wave climate, possible river inflow and the type of sediment available [*Officer*, 1976]. Besides a large variability in size and shape of embayments, also the characteristics of the main elements, the channels, tidal flats and salt marshes, differ widely. Broadly speaking two different channel patterns can be discerned, viz. braiding and branching patterns [*van Veen*, 1950]. Braiding patterns are commonly found in elongated, shallow embayments, such as the Western Scheldt in the Netherlands [*Jeuken*, 2000], and the Humber in the UK. Branching patterns typically occur in short and wide tidal basins. The large inlet channel of these tidal basins branches into smaller channels, which branch in their turn into yet smaller ones. Many examples of well-developed branching channel patterns are found in salt marshes, e.g., the Venice Lagoon in Italy, on the North Norfolk coast in the UK, and in San Francisco Bay and Massachusetts Bays, USA. Tidal networks draining unvegetated tidal flats are more scarce (e.g., Dutch and German Wadden Sea [*Oost*, 1995]).

[4] Recent developments for automatic extraction of the tidal channel network from digital terrain maps of marsh and tidal flat lands [*Fagherazzi et al.*, 1999] have improved the possibilities to study these systems [*Rinaldo et al.*, 1999a, 1999b]. Using this technique, it was shown that tidal networks exhibit great variety in their geometrical and topological form, and channel networks in different tidal basins exhibit quite different overall scaling characteristics [*Fagherazzi et al.*, 1999a; *Rinaldo et al.*, 1999a].

[5] Significant field-based descriptions concerning branching patterns in salt marshes (see *Allen* [2000] for a quite complete review and *Friedrichs and Perry* [2001]) have added much to our knowledge of these systems. New tools are now available for quantitative and qualitative description of these patterns [*Marani et al.*, 2003].

[1] Also at Dipartimento Ingegneria Idraulica Marittima Ambientale e Geotecnica, Universitá di Padova, Padova, Italy.
[2] Also at WL/Delft Hydraulics, Delft, The Netherlands.

0148-0227/05/2003JF000092$09.00

[6] On the contrary, despite the great amount of observational data, well-assessed analysis tools to quantitatively describe characteristics of branching channel patterns in the deeper, more sandy tidal environments are scarce. These patterns are expected in basins that are short compared to the tidal wave length and with comparable length and width. Though this type of inlet is commonly observed around the US coast, most of these lagoons are "drowned" inlets in which the channel pattern outside the flood delta is poorly developed (e.g., Redfish Pass, Florida and Shinnecock Inlet, New York).

[7] The well-developed channel patterns in six basins of the Dutch Wadden Sea were investigated by *Cleveringa and Oost* [1999], who found that all systems in the Wadden Sea consist of similar three- to four-times branching networks. The branch lengths decrease logarithmically, but do not continue below the 500 m scale in the data considered.

[8] Besides observations, models are useful tools to study these channel systems. Many models have been developed for estuarine morphodynamics [see, e.g., *De Vriend*, 1996; *De Vriend and Ribberink*, 1996]. These models are largely semiempirical, or restricted to one-dimensional approximations. *Fagherazzi and Furbish* [2001] developed a model that simulates aspects of initial channel formation in a salt marsh and studied the evolution of the shape of a reference cross section that includes an incipient channel zone and a marsh surface zone. *Lanzoni and Seminara* [2002], using a one-dimensional model, showed that a tidal channel in equilibrium has a concave profile. However, for a two-dimensional flow in a short tidal basin, the flow is directed almost radially to and from the inlet and the resulting equilibrium profile for the shallows and the channels can be far different from the 1D case. Using a formally integrated long-term model, *Schuttelaars* [2000] showed that in areas with unvegetated tidal flats stable morphodynamic equilibra exist. The bottom patterns resemble natural branching channels. Furthermore, it is shown that multiple equilibra can occur, i.e., under the same conditions different morphodynamic equilibra can exist. In this approach the temporal behavior of a finite number of fixed spatial patterns is described by a nonlinear evolution equation. The spatial patterns result from a linear stability analysis. Owing to the limitation in the number of bottom patterns, the morphodynamic behavior was only investigated for values of the friction parameter much smaller than those observed. In contrast, numerical simulation of tidal channel network development based on numerical integration of mass, momentum, and sediment balance equations is still lacking.

[9] The main objective of this paper is to present a numerical model based on a set of two-dimensional equations for water motion, sediment transport and bed level changes capable of reproducing branching channel patterns. In addition, we present a linear stability analysis of branching channel patterns in a tidal environment based on a simplified set of equations derived from the ones used in the numerical model. These models are validated against each other, as well as against field data available.

[10] The different approaches are described in the following sections. First a linear stability analysis is introduced, which leads to a relationship between the number of channels per unit span width and some physical parameters of the tidal system. The subsequent section describes the setup of the process-based numerical model for a geometrically simplified basin and the channel pattern resulting from the simulation. Next the results of these two approaches are compared mutually and with available experimental data from the Dutch Wadden Sea. In the final discussion, attention is paid to shortcomings of the theoretical and model approaches, the sensitivity of the results to physical parameters and how to "translate" model results to field data. Finally, the main conclusions are summarized in section 7.

2. Mathematical Formulations

[11] The water motion in the models is described by the unsteady depth-averaged shallow water equations in two dimensions. The depth and density averaged momentum equations in x and y direction are given by

$$\frac{\partial u}{\partial t}+u\frac{\partial u}{\partial x}+v\frac{\partial u}{\partial y}+g\frac{\partial \eta}{\partial x}-fv+\frac{gu|U|}{C^2h}-\frac{F_x}{\rho_w h}-\nu\left(\frac{\partial^2 u}{\partial x^2}+\frac{\partial^2 u}{\partial y^2}\right)=0 \quad (1)$$

$$\frac{\partial v}{\partial t}+u\frac{\partial v}{\partial x}+v\frac{\partial v}{\partial y}+g\frac{\partial \eta}{\partial y}+fu+\frac{gv|U|}{C^2h}-\frac{F_y}{\rho_w h}-\nu\left(\frac{\partial^2 v}{\partial x^2}+\frac{\partial^2 v}{\partial y^2}\right)=0. \quad (2)$$

[12] The corresponding mass balance equation is given by

$$\frac{\partial \eta}{\partial t}+\frac{\partial hu}{\partial x}+\frac{\partial hv}{\partial y}=0, \quad (3)$$

in which

C Chézy coefficient [$m^{1/2}/s$],
h water depth = $z_b + \eta$ [m],
η water level [m],
z_b bed level [m],
f Corioli's parameter [1/s],
$F_{x,y}$ x and y component of external forces [N/m^2],
u, v depth averaged velocity [m/s],
U absolute magnitude of total velocity, $U = (u^2 + v^2)^{1/2}$ [m/s],
ρ_W mass density of water [kg/m^3],
ν effective diffusion coefficient (eddy viscosity) [m^2/s].

[13] The sediment transport is described using the formulation of *Engelund and Hansen* [1967], where the sediment rates are calculated as total load (s), according to

$$s=\frac{0.05\alpha U^5}{g^{0.5}C^3\Delta^2 d_{50}}\left(1-\beta\frac{\partial z_b}{\partial \xi}\right), \quad (4)$$

where

α calibration coefficient;
Δ the relative density $(\rho_s - \rho_w)/\rho_w$;

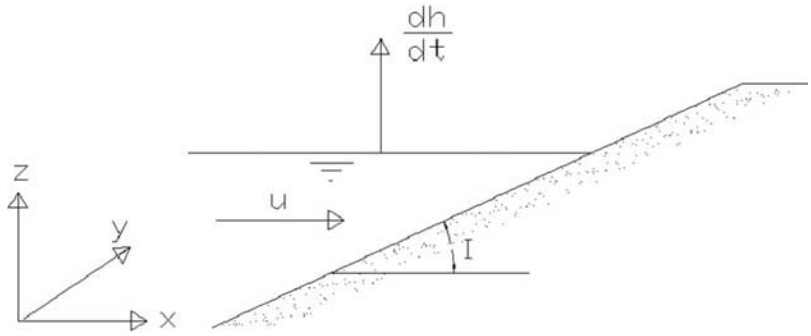

Figure 1. Definition sketch used in the theoretical analysis.

d_{50} characteristic grain size [m];
ξ coordinate along-flow direction [m].

[14] Bottom level changes follows due to conservation of sediment mass:

$$\left(1-\varepsilon_{por}\right)\frac{\partial z_b}{\partial t}+\left(\frac{\partial s_x}{\partial x}+\frac{\partial s_y}{\partial y}\right)=0, \tag{5}$$

in which

ε_{por} bed porosity;
s_x, s_y sediment transport in x and y direction [m^3/m/s]:

$$s_x = s\cos\alpha \qquad s_y = s\sin\alpha. \tag{6}$$

[15] The direction α of the sediment transport depends on the direction of the bed shear stress δ and the bed slope:

$$\tan\alpha = \frac{\sin\delta - \dfrac{1}{f_s\theta}\dfrac{\partial z_b}{\partial y}}{\cos\delta - \dfrac{1}{f_s\theta}\dfrac{\partial z_b}{\partial x}}, \tag{7}$$

where θ is the Shields parameter and f_s is an efficiency factor for the downhill gravitational transport, having a value between 1 and 2. For calculating the direction of the bed shear stress δ the influence of secondary flow is taken into account:

$$\delta = \arctan\left(\frac{v}{u}\right) - \arctan\left(A\frac{h}{R}\right). \tag{8}$$

[16] The second term in this equation represents the influence of the secondary flow. A is a coefficient and R is the effective curvature [see *Struiksma et al.*, 1985].

3. Theoretical Analysis

[17] The theoretical analysis presented here is presented first in *Wang* [1992]. Because this publication is difficult to obtain, the analysis is presented below. The starting point of the theoretical stability analysis is the basic set of equations governing the flow, sediment transport and morphological development as given in equations (1)–(5). First a basic state is defined as the zero-order solution. For this purpose we use the situation as outlined in Figure 1, i.e., a plane sloping bottom with vanishing depth at the end of the basin. This situation is a quasi-equilibrium state under the assumption that the length of the embayment is much smaller than the tidal wave length. With this assumption the water level is in phase throughout the model domain and becomes a function of time only. The flow velocity at every point in time is constant throughout the model domain:

$$u(t,x,y) = \frac{1}{I}\frac{\partial \eta}{\partial t}, \tag{9}$$

where I is the bottom slope in the basic state. Note that the landward boundary is a moving boundary and its moving velocity is equal to the expression given in equation (9). The equilibrium condition is satisfied in the whole flooded area, since

$$\frac{\partial s_x}{\partial x} = \frac{ds}{du}\frac{\partial u}{\partial x} = 0 \qquad s_y = 0. \tag{10}$$

[18] Only at the moving landward boundary can sedimentation (during flood) or erosion (during ebb) occur. It is noted that this is not always a true morphological equilibrium, because the residual sediment transport does not necessarily vanish. The latter is only the case if the tide is symmetric. Otherwise sedimentation or erosion will take place on the intertidal area, while in the channels (submerged during the whole tidal period) the bottom does not change. For the present infinitesimal perturbation analysis, the plane sloping bottom represents a near-equilibrium state and is therefore used as a zero-order solution in the linear analysis. On the basis of a more formal analysis, *Schuttelaars and de Swart* [1996] derived a morphological equilibrium state for short tidal embayments that appears to be almost linear [see also *Lanzoni and Seminara*, 2002].

[19] The zero-order solution is thus

$$h = h_0(x), \quad u = u_0 = \frac{1}{I}\frac{\partial \eta}{\partial t}, \quad v = 0. \tag{11}$$

[20] Note that the zero-order solution for water depth h_0 is a function of x (Figure 1), whereas that for the longitudinal velocity u_0 is not. Using this zero-order solution implies that the analysis only applies for short and semiclosed basins.

[21] The first-order solution is obtained by superimposing a small perturbation (h', u', v') onto the zero-order solution. Here the same linearization is applied as in *Struiksma et al.*

[1985]. Time derivatives in the equations have been ignored, i.e., a quasi-steady state is considered:

$$\frac{\partial}{\partial y}\left[u_0\frac{\partial u'}{\partial x}+\frac{g}{C^2}\frac{u_0^2}{h_0}\left(2\frac{u'}{u_0}-\frac{h'}{h_0}\right)\right]-\frac{\partial}{\partial x}\left[u_0\frac{\partial v'}{\partial x}+\frac{g}{C^2}\frac{u_0}{h_0}v'\right]=0, \tag{12}$$

$$h_0\frac{\partial u'}{\partial x}+h_0\frac{\partial v'}{\partial y}-u'I+u_0\frac{\partial h'}{\partial x}=0, \tag{13}$$

$$\frac{b}{u_0}\frac{\partial u'}{\partial x}+\frac{\partial}{\partial y}\left[\frac{v'}{u_0}+A\frac{h_0}{u_0}\frac{\partial v'}{\partial x}+\frac{1}{f_s\theta}\frac{\partial h'}{\partial y}\right]=0. \tag{14}$$

[22] In equation (12) the pressure term has been eliminated by cross differentiating the two momentum equations and subtracting the results. In the present case, h_0 is a function of x, which leads to an extra contribution to this last term on the left hand side of the equation. In equation (13), an extra term with the slope I appears, due to the plane sloping zero-order bottom. Equation (14) is the same equation as in the analysis of *Struiksma et al.* [1985]. It says that, also in the perturbed situation, there are no transport gradients. This means that the analysis investigates the possible existence of a perturbed equilibrium state. The term with $f_s\theta$ in equation (14) originates from the bed slope effect on the sediment transport (equation (7)). The parameter b is a sediment transport parameter, which originates from the linearization of the sediment transport formula:

$$b=\frac{u_0}{s_0}\frac{\partial s_0}{\partial u_0}. \tag{15}$$

[23] It is assumed to be constant. It implies that the sediment transport formula is approximated by a power of the flow velocity (for equation (4)b is exactly equal to 5).

[24] Ignoring the time derivatives can be justified as follows. The time derivative of the water level in equation (3) is the driving force of the system and it is balanced in the zero-order approximation. The time derivative in the perturbation to the mass balance equation for water (equation (13)) will thus always vanish. The time derivatives of the flow velocities in the momentum equations can be neglected near maximum flood and maximum ebb flow. This means that neglecting the time derivatives in these equations is equivalent to assuming that the morphology of the system is controlled by the periods with the highest flow velocity.

[25] Substituting the following harmonic perturbation,

$$\begin{pmatrix}h'\\u'\\v'\end{pmatrix}=\begin{pmatrix}H\\U\\V\end{pmatrix}\exp\left(ik_x x+ik_y y\right), \tag{16}$$

into the system of equations leads to a relation between the two complex wave numbers k_x and k_y:

$$\begin{aligned}b(ik_x)^4&+\left[\left(Ah_0-\frac{h_0}{f_s\theta}\right)(ik_y)^2+\frac{bg}{C^2h_0}\right](ik_x)^3\\&+\left[1+3A\frac{g}{C^2}+\frac{I-\frac{g}{C^2}}{f_s\theta}\right](ik_x)^2(ik_y)^2\\&+\left[(3-b)\frac{g}{C^2h_0}-\frac{h_0}{f_s\theta}(ik_y)^2-\frac{g}{C^2}\frac{I}{h_0}\left(A-\frac{1}{f_s\theta}\right)\right]\\&\cdot(ik_y)^2ik_x+\left[\frac{2g}{C^2}\frac{1}{f_s\theta}(ik_y)^4+\frac{gI}{C^2h_0^2}(ik_y)^2\right]=0.\end{aligned} \tag{17}$$

[26] As compared to the corresponding equation derived by *Struiksma et al.* [1985], there are two important differences: (1) in the analysis of *Struiksma et al.* [1985] the impermeable walls put constraints on the transverse wave number k_y, which is not the case here; (2) in the above equation extra terms are present because of the bed slope I.

[27] The second difference has an important consequence. For the case $k_x = 0$, *Struiksma et al.* [1985] would find the trivial solution $k_y = 0$, but for the present case an additional nontrivial solution is found for k_y:

$$(k_y h_0)^2=\frac{If_s\theta}{2}. \tag{18}$$

[28] Note that in equations (17) and (18) the extra term due to the bed slope in equation (12) is ignored. If this term were included, the solution would read

$$(k_y h_0)^2=\frac{If_s\theta}{2}-\frac{I^2}{2}. \tag{19}$$

[29] However, the last term in this equation is negligible, as $I \ll f_s\theta$. Therefore equation (18) will be used henceforth.

[30] It is noted that $k_x = 0$ means that the perturbation is neither decreasing nor increasing in the x direction, i.e., along the channels (wave troughs of the k_y waves). Such a perturbation is more stable than any other one with $k_x \neq 0$, because the flow direction is continuously changing in tidal regions. Therefore the transverse wave according to equation (18) is presumably a dominant mode and it should say something about the channel configuration in tidal areas.

[31] The following observations are made from the expression of the dominant wave number: (1) the larger the slope I, the smaller and more closely spaced the channels; (2) the more morphologically active the region (larger Shields parameter), the smaller and more closely spaced the channels; (3) the larger the water depth the larger and more widely spaced the channels.

[32] It is furthermore interesting to note that in a certain area the undisturbed water depth varies continuously in space, whereas the wave number does not, since only a discrete number of waves may occur. Every time a bifurcation occurs the wave number is doubled. According to equation (18), doubling of the wave number can happen if the undisturbed water depth is halved. Note that this conclusion does not depend on the assumption of constant bed slope. For the constant bed slope, this means that the channels beyond a bifurcation have half the length of the channel before it. The lengths of the channels thus decrease exponentially with the order of bifurcations, as shown in Figure 2. The structure shown in Figure 2 is a Cantor's tree, which is an example of a fractal structure.

[33] Furthermore, it is important to note that the term representing the influence of the secondary flow does not influence the dominant wave number (equation (18)). This implies that for reproducing the branching channel structure it is not necessary to take into account the secondary flow effects.

4. Numerical Model

4.1. Model Description

[34] The numerical modeling system used herein is Delft3D, developed by WL/Delft Hydraulics [*Roelvink*

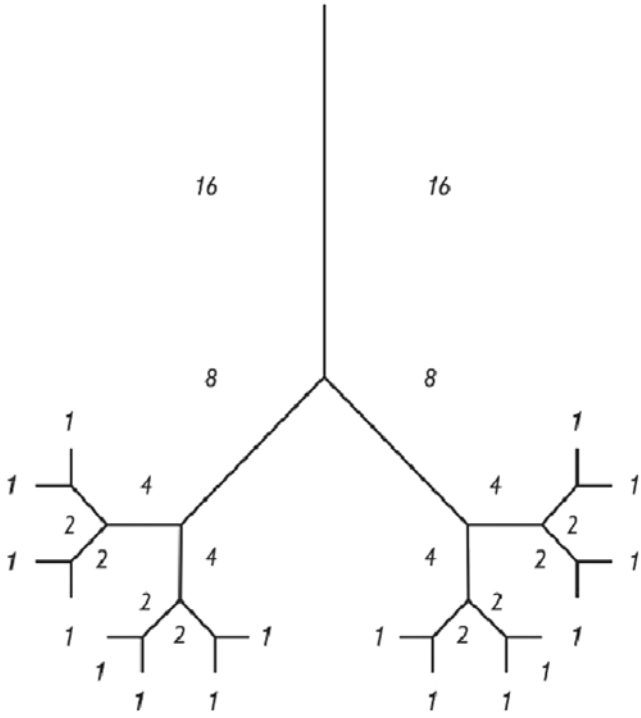

Figure 2. Theoretical tree structure or Cantor's tree. The lengths of the channels decrease exponentially with the order of bifurcations.

and van Banning, 1994; *Wang et al.*, 1991, 1995]. Delft3D is a finite difference numerical modeling system composed of a number of modules describing waves, currents, sediment transport and bottom changes, which are linked in a steering module. The flow module provides the hydrodynamic basis for morphological computations. It computes the tidal flow by solving the unsteady depth-averaged shallow water equations in two dimensions (equations (1)–(3)) with an Alternating Direction Implicit (ADI) technique [*Stelling*, 1984]. In tidal areas, shallow parts can fall dry during part of the tidal cycle. In the flow module, this flooding and drying is represented by removing grid cells that become dry when the tide falls, and reactivating cells that become wet when the tide rises. If the total water depth in a velocity point is below a certain threshold (0.1 m), this point is set dry, which means that the local velocity is set equal to zero.

[35] The transport computations, based on the time-dependent flow fields, are carried out in the transport module, which gives access to a variety of semiempirical formulae. In this model the total sediment transport formula of Engelund and Hansen (equation (4)) is applied. In the bottom module, the bathymetry is updated from the divergence of the tidally averaged sediment transport field (equation (5)), using an explicit scheme of the Lax-Wendroff type.

[36] In this study, the flow module is called for one tidal period, with a time step of 1 min, followed by a transport computation for this tidal period with a time step of 10 min. The bottom module applies the averaged transport field over the morphological time step, which is usually much larger than one tidal period. The morphological updating is done with an automatic time stepping procedure. This process loop is repeated with every updated bathymetry, until the prescribed stopping time is reached.

4.2. Model Setup

[37] The model uses a schematic representation of a tidal basin. The simplifications make it possible to investigate the development of channel patterns in general [cf. *Hibma et al.*, 2003a], and to make a comparison with the theoretical analysis. Model parameters correspond with those in the tidal basins in the Dutch Wadden Sea. Wind waves are not accounted for and therefore this model represents a tide-dominated basin in the mesotidal category of *Hayes* [1975].

[38] A rectangular model grid is used in the numerical computation. In order to combine a manageable computation time with a sufficient resolution of the basin morphology, a grid size of 100 m is adopted. The model covers an area of 12 * 16 km and is composed of an offshore area extending 4 km seaward and an inner basin of 8 * 16 km. The areas are divided by thin dams, representing barrier islands (see Figure 3).

[39] The cross-sectional area of the inlet channel (A_c) between the islands fulfils *O'Brien*'s [1969] empirical relationship with the tidal prism (P), $A_c = c \cdot P$ where $c = 6.6 * 10^{-5}$ for the Wadden Sea [*Biegel*, 1991].

[40] The boundaries enclosing the inner basin are fixed and impermeable. At the seaward boundary a harmonically varying water level is imposed, with a constant phase along the boundary. It represents a semidiurnal tidal fluctuation, with an amplitude of 1 m. Higher-order components are induced by friction and interaction during the propagation of the tidal wave through the model area.

[41] The distribution of channels, flats and marshes inside the basin can be described by the hypsometric curve of the basin, which gives the surface area per bed level interval. From the hypsometric distribution for the Wadden Sea an initial bathymetry for the model simulation is derived, in which channel and shoal patterns are not yet developed. Figure 4 shows this hypsometry for a parabolic bottom profile, which decreases from MSL −6 m in the inlet to MSL +1 m at the landward boundary.

[42] In the offshore area there is initially a plane sloping coast between MSL −8 m at the seaward boundary to MSL −6 m at the inlet.

[43] The initial bed level in the basin is given random small-amplitude perturbations, by adding a random value to the depth value of each grid cell. These initial disturbances maximally amount to plus or minus 15 cm.

[44] The bed material consists of uniform sand with D_{50} = 120 μm. For the bottom roughness, a Chézy value of 65 $m^{1/2}/s$ is used. The Corioli's force is neglected, while the three dimensional effect of secondary flow in the two-dimensional depth-averaged simulation is accounted for using a parametric secondary flow model.

4.3. Model Results

[45] The model simulation covers a time span of 100 years. Owing to the equilibrium profile adopted, the first significant changes in the bathymetry occur rapidly and after about 10 years the ebb-tidal delta in the offshore area is already clearly recognizable. After 30 years, the flood-tidal delta also developed: the scouring of the inlet has resulted in the

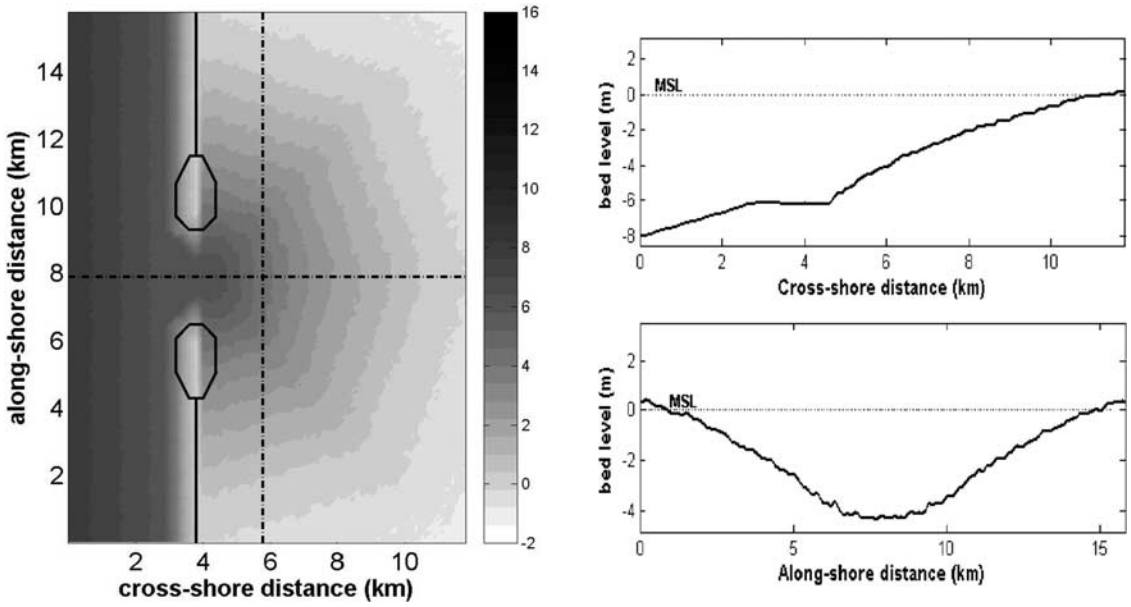

Figure 3. Initial bathymetry for the model simulation (top view and cross sections). A parabolic bottom profile represents a quasi-equilibrium configuration on which channel and shoal patterns are not yet developed, according to the hypsometric distribution of the Wadden Sea.

formation and deepening of a large ebb-dominated main channel and of two lateral flood channels through the inlet, which subsequently branch into smaller channels in their turn.

[46] This initial channel network gradually evolves into a complex branching channel shoal pattern that covers in about one century the whole surface of the inner basin, as shown in Figure 5. In this case we observe a well-developed flood-tidal delta encompassing the entire basin, like in the Wadden Sea and in the Venice Lagoon, for instance.

[47] During this evolutional stage the inlet has deepened from an initial depth of 6 m below MSL to a maximum depth of 18 m and the cross-sectional area has increased from an initial value of $13 \cdot 10^6$ m^2 to $18 \cdot 10^6$ m^2. The smallest recognizable channels have a mean depth of about 1.5 m below MSL draining an area with a depth of approximately 0.5m.

[48] From a quantitative analysis of the cross-shore velocities averaged over a tidal cycle, it is possible to distinguish the alternating ebb and flood dominance over the basin. The inlet gorge turned out to be slightly ebb-dominated. This is consistent with the overall erosion trend: the mean depth of the basin increases from 1 m below MSL to 1.2 m below MSL.

[49] From sensitivity simulations with the numerical model it appeared that the initial bottom profile has an essential influence on the development of the channel pattern. If the initial sediment distribution over the basin agrees with observations of basins in equilibrium (Figure 7), the model yields a well-developed channel system. On the other hand, deviations from this initial equilibrium hypsometry lead to locally underdeveloped channel patterns. In the case of a linear initial profile, for instance, an underdeveloped flood delta emerges, characterized by a relatively deep basin where channels are only formed in the shallower areas along the watersheds (see Figure 6). This type of basin is also observed in nature, e.g., Shinnecock Inlet, New York, USA. Shinnecock Inlet was formed during a hurricane when high waves and a storm surge overwashed the barrier. The fact that the adjacent Shinnecock Bay was wide and relatively deep aided the development of the inlet system and the eroded barrier sand started washing into the inlet enlarging the flood-tidal delta (from US Army Corps of Engineers, http://www.oceanscience.net/inletsonline).

[50] The spatial development of channel structure can also be related to the timescales involved. The adaptation of the sediment budget over the entire basin, in order to establish an equilibrium profile, is a spatially large-scale process, which involves large timescales. The local formation of channel structures is associated with smaller timescales. However, for the development of a channel structure

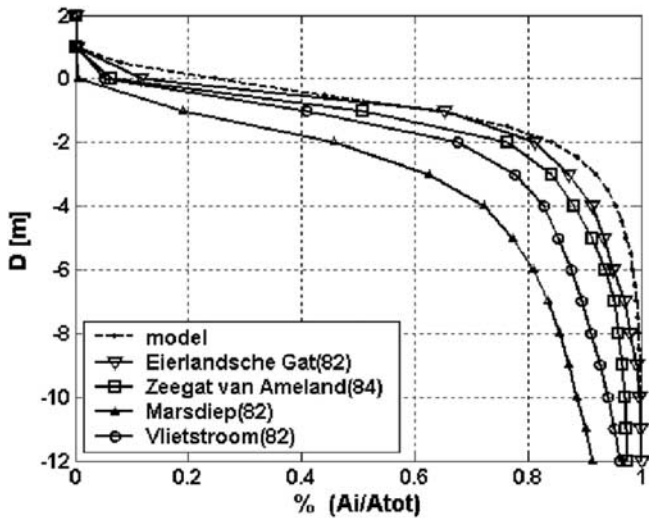

Figure 4. Hypsometric curves of the model and some representative basins in the Wadden Sea.

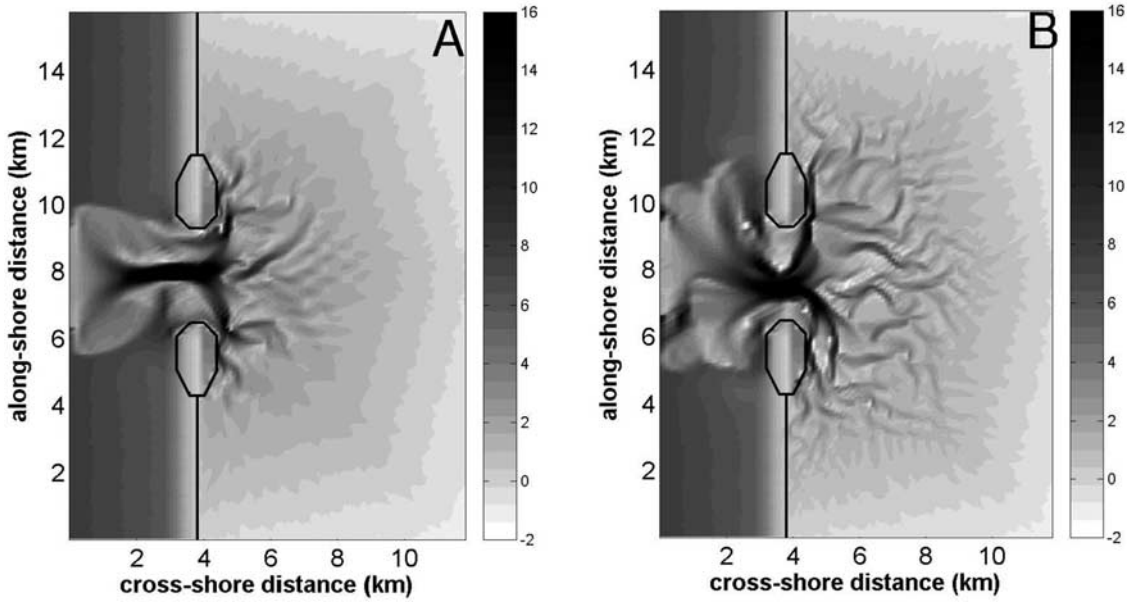

Figure 5. Results of the model simulation after (a) 30 and (b) 100 years.

sediment needs to be transported in the lateral direction. The transport capacity in this direction is initially much smaller than in the longitudinal direction. Therefore the process may involve a long time if much sediment needs to be moved for the large-scale adaptation of the hypsometry. Thus the pattern formation is slowed down at locations where the underlying profile strongly deviates from the equilibrium state. Sensitivity analysis showed that parameters influencing the timescales of the model, like sediment grain size, sediment transport formulation and amplitude of the imposed water level variation, have no discriminating influence in space and therefore do not determine the emerging channel pattern.

[51] The channel pattern formed near the borders of the basin, as observed in Figure 6, show that the channel formation does not only originate from an ongoing branching starting from the main channel through the inlet, but also develops from locally growing undulations merging into a channel system. The latter process was also observed for the emergence of braiding channel patterns in elongated estuaries [*Hibma et al.*, 2003a].

5. Validation of Model Results

[52] In this section the results of the theoretical analysis and numerical model are validated by mutual comparison and by comparison with field observations. First the agreement between numerical model results and natural branching patterns is tested using Horton's hierarchical analysis. This analysis technique forms a simple tool to characterize the properties of branching patterns. Then the theoretical analysis is compared with field observations. Finally the validity of the theoretical relation (equation (18)) for the numerical model results is investigated, closing the loop of intercomparison of all approaches presented.

5.1. Numerical Model Results and Field Data

[53] *Horton* [1945] devised geometric scaling relationships between the stream numbers, lengths, and drainage areas of channels in networks. Horton's hierarchical analysis starts with the definition of the smallest channels as first-order channels. The confluence of two first-order channels defines a second-order channel, and so on (Figure 7). The confluence of a lower-order channel with a higher-order channel does not change the order of either of them. The analysis is accomplished by simply counting the number of first-, second- and higher-order channels. According to Horton's theory the number of channel branches in fractal

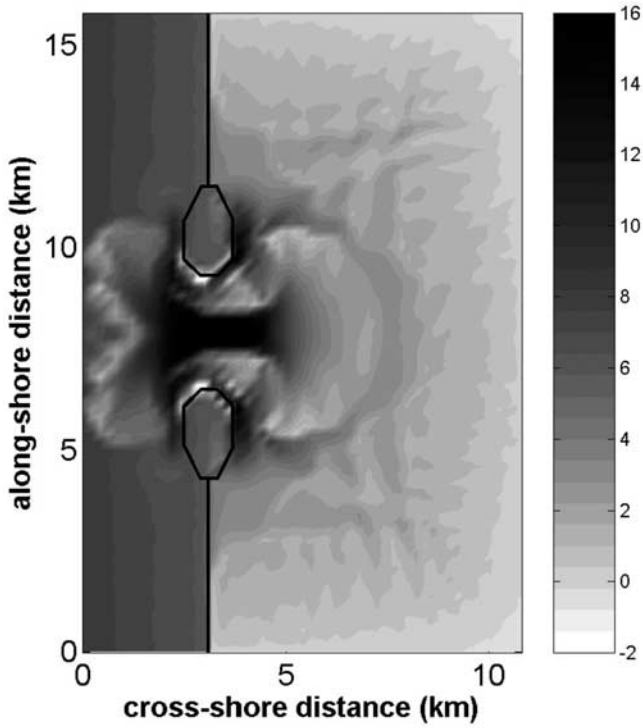

Figure 6. Results of the model simulation starting from a linear profile after 100 years.

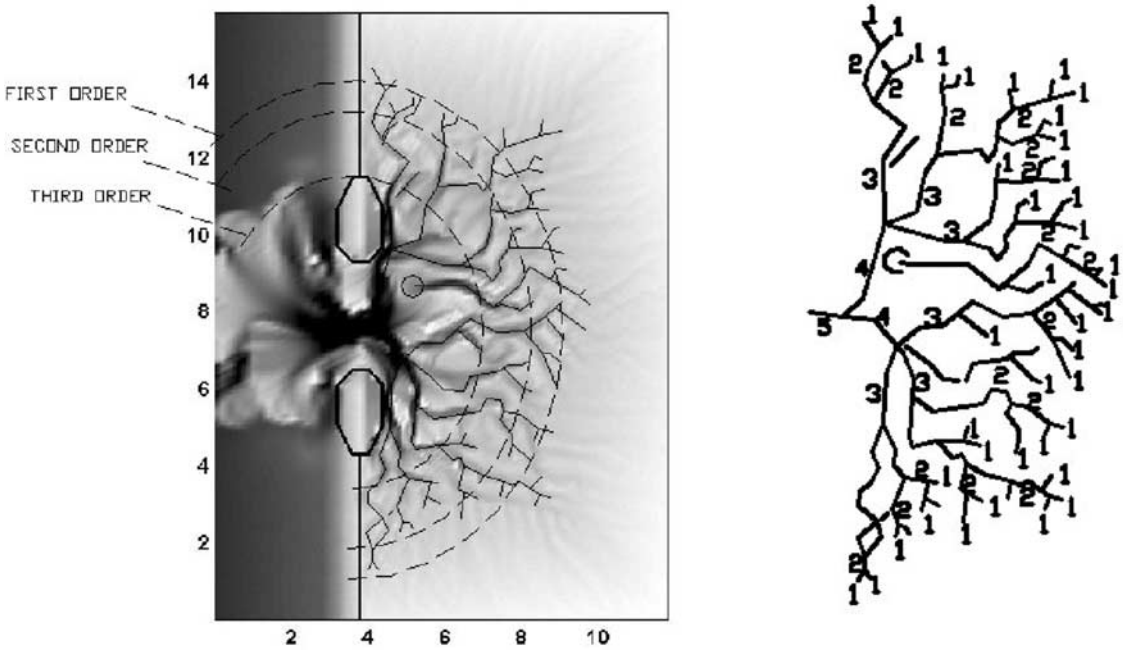

Figure 7. Hierarchical analysis of model results using Horton structure orders. The smallest channels are defined as first-order channels, then second, third, fourth, and fifth orders follow.

patterns increases logarithmically with decreasing channel order.

[54] Using Horton's definition, the order of the channels in the model result is determined. Figure 7 shows these first-, second-, third-, and fourth-order branches. Subsequently, the number of channels of each order is counted and plotted logarithmically against their order number (see Figure 8). In agreement with Horton's hierarchical analysis the number of channel branches increases logarithmically with decreasing channel order. The theoretical three- and four-times branching networks are indicated, as well. The model simulation displays a three-times branching pattern, as can be observed from the slope of the curve in Figure 8 and from the channel scheme in Figure 7 (right panel).

[55] *Cleveringa and Oost* [1999] applied Horton's hierarchical analysis to the channel networks of the Wadden Sea. Their results are shown in Figure 8 (right panel). As in the plot from model simulation data, all investigated channel systems display a similar logarithmic relation between the channel order and the number of channels of that order, as indicated by the similarity in the slope of the fits. The position of the channel systems relative to each other is determined by their size: small systems have fewer channels than large ones. The curves of the Wadden Sea networks vary between those for a three-times and a four-times branching network, with a slight preference for the latter.

[56] The slopes of the lines representing the branching pattern in the simulation and those in the Wadden Sea agree

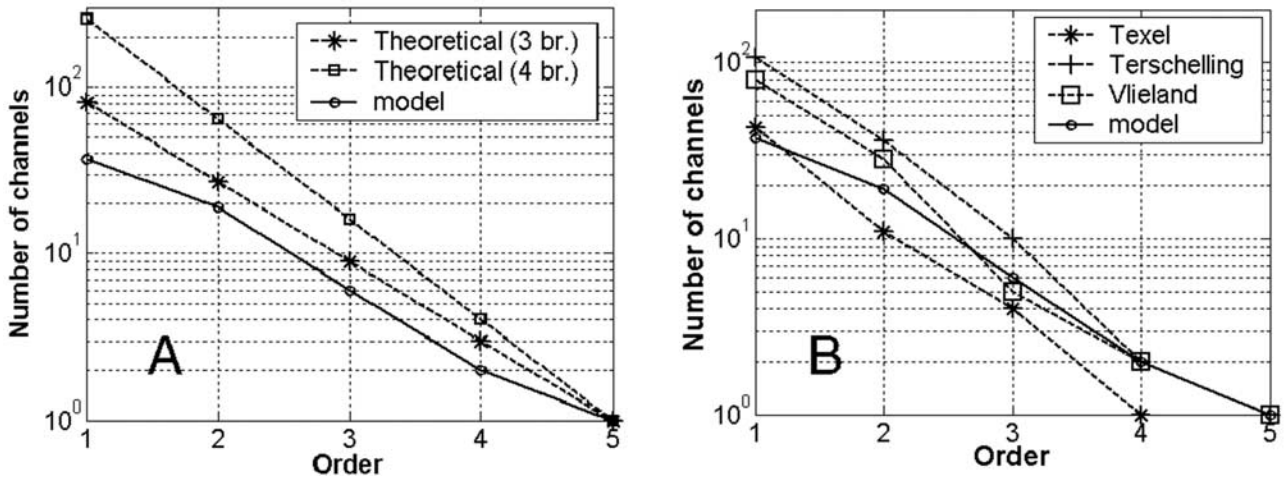

Figure 8. Number of channels of each order compared with (a) fits of the theoretical three- and four-times branching networks and with (b) example basins of the Wadden Sea. The number of channel branches increases logarithmically with decreasing channel order.

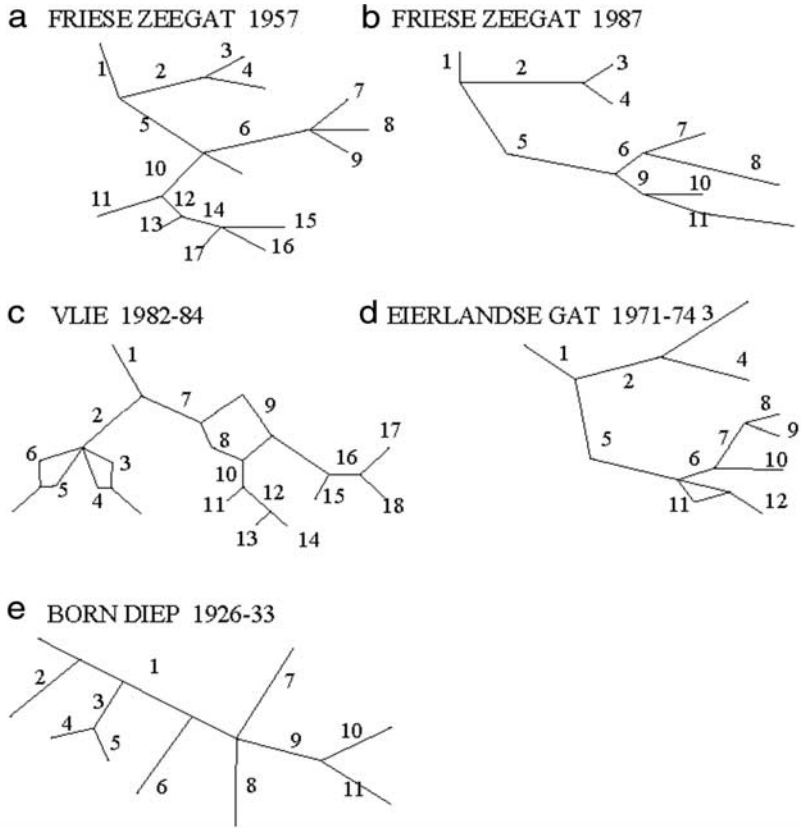

Figure 9. Channel structure for four basins of the Wadden Sea ((a, b) Friesche Zeegat, (c) Vlie, (d) Eierlandse Gat, and (e) Born Diep) derived from the bathymetric data.

well with the theoretical lines, irrespective of the size of the systems, the tidal prism or the intertidal flats. This indicates that the model is able to reproduce the branching patterns of natural channel networks, satisfying Horton's law. A comment given on Horton's hierarchical analysis is that it is not very discriminating for fractality assessment, because properties proposed by Horton as bifurcation and length ratio of successive stream orders have values that inevitably occur for channel networks [*Kirchner*, 1993; *Rodriguez-Iturbe et al.*, 1994; *Rinaldo et al.*, 1999a; see also *Fagherazzi et al.*, 1999]. Therefore we restrict the analysis to an indication of the branching order.

5.2. Theoretical Analysis and Field Data

[57] The results from the theoretical analysis have been tested against field data from the Dutch Wadden Sea by *Fokkink* [1993]. For four basins (Friesche Zeegat, Vlie, Eierlandse Gat and Born Diep) he derived the channel structures from the bathymetric data, as shown in Figure 9. Note that for the Friesche Zeegat two situations have been considered, i.e., before (1957) and after (1987) the closure of Lauwerszee in 1969 (see Figure 10). For each of the channels indicated in these figures the channel width, the channel depth and the averaged bottom slope along the channel have been determined from the field data (Table 1).

[58] In Table 2 the statistics of two parameters have been given for the five cases considered: the ratio between channel depths after and before bifurcations, and the parameter h^2/B^2I. Theoretically, the first parameter should be constant and equal to 0.5. The second parameter should be constant according to equation (18) if the channel width is taken as a proxy of the wave length. It is further noted that for the parameters h and I the values of the channels have been used instead of those in the undisturbed condition, because it is difficult to construct the undisturbed state from the field data.

[59] The results shown in Table 2 indicate that the first parameter is indeed about 0.5, i.e., the channel depth is halved after each bifurcation. Only the case of the Friesche Zeegat in 1987 shows a large deviation. Apparently this indicates that this basin in 1987, i.e., 18 years after the closure of the Lauwerszee, had not yet achieved its new morphological equilibrium state. This is supported by the fact that the deviations especially occur in those branches where the largest morphological changes are still taking place, i.e., branches 5, 8, 9, 10, 11. Similar conclusion can be drawn about the second parameter, although the scatter is much larger. Note that the channel width has been used in this parameter instead of the wavelength. This is possibly an explanation why the scatter in this parameter is larger. Apparently the conclusion that the channel depth halves at a bifurcation is best supported by the field data. It is noted that this conclusion directly follows from the result of the analysis (equation (18)). We note that this result of the stability analysis concerning the initial pattern appears to apply well to the natural state (beyond the linear domain). A possible explanation is that the result of the analysis does not concern the fastest growing (in t or x direction) mode,

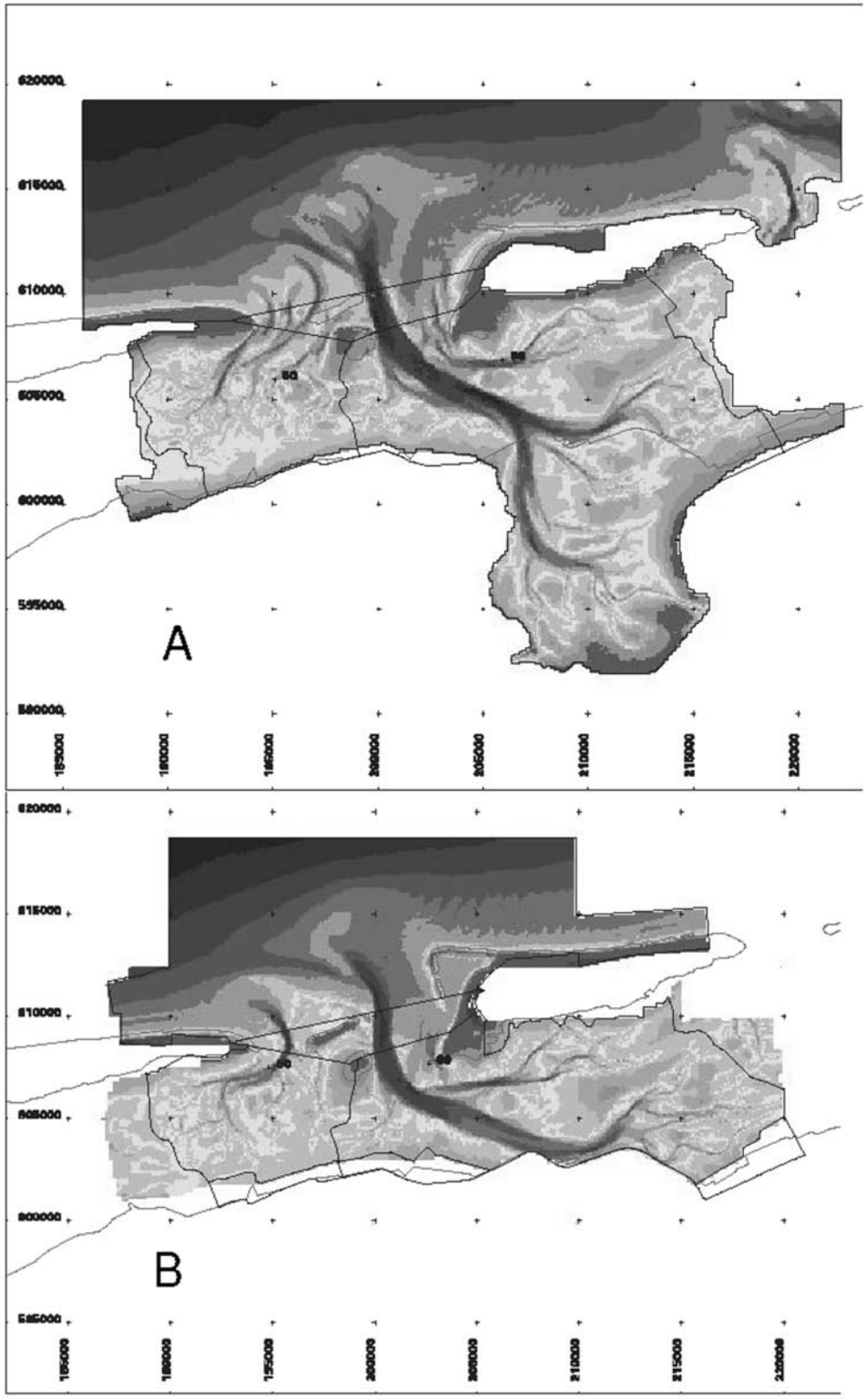

Figure 10. Bathymetry of the Friesche Zeegat in 1957, i.e., (a) before, and in 1987, i.e., (b) after, the 1969 closure of the Lauwerszee [from *Biegel*, 1993]. See color version of this figure in the HTML.

but the mode which does not grow nor decay in the x direction.

5.3. Theoretical and Numerical Model Results

[60] The relationship between the number of channels per unit span width and the physical parameters of the system as given in equation (18) is investigated for the channel system resulting from the numerical model.

[61] In the model a constant value of D_{50} is used. The velocities over the basin are assumed to be uniform for the equilibrium profile [*Friedrichs and Aubrey*, 1996; *Schuttelaars and de Swart*, 1996; *Lanzoni and Seminara*,

Table 1. Collected Data From Dutch Wadden Sea[a]

	Friesche Zeegat 57			Friesche Zeegat 87			Vlie			Eierlandse Gat			Born Diep		
Channel	B, m	h, m	$I \times 1000$	B, m	h, m	$I \times 1000$	B, m	h, m	$I \times 1000$	B, m	h, m	$I \times 1000$	B, m	h, m	$I \times 1000$
1	1300	20	5										1500	18	2.5
2	800	8	2.3	750	7.5	2.6	2000	17	2.8	1500	5.5	1.6			
3	600	5	7	250	6.5	3.2	1000	11	2	750	5	0.6			
4	350	4	10	300	9.5	2.7	1000	9	1.5	750	6	1.3			
5	1500	17	6	1500	11	1.5	1250	13	2.4	1500	7	2.5			
6	1000	11	3	300	9	6	1500	11	2	500	2.5	4	750	7	3
7	500	5	8	350	3.5	4	2000	14	5.3	750	5	2.3	1000	5	3
8	500	4	2.3				1750	14	1.2	1000	6	2	1250	5	1.3
9	1000	3	4.9				750	11	1.2	750	6	1	1500	9.5	3
10	1000	13	4.5	300	8	2				500	2	1	1500	5.5	1.3
11	500	6	26	150	3	1.5	750	4.5	3	400	2	1	1000	7	1.7
12	1000	7	6.3	350	5	5	750	6.5	1.1	750	3.5	1.3			
13	700	4	2.5				500	3	1.3						
14							750	2.5	1.4						
15	500	4	1.8				1000	6.5	3.5						
16	250	5	1.8				800	5	4.4						
17	250	3	2												

[a]After *Fokkink* [1993]. Channel number in the first column is indicated in Figure 9. B, width of channel; h, depth of channel; I, slope along channel.

2002; *Pritchard et al.*, 2002]. This implies a constant shape factor and Shields parameter. Then equation (18) can be expressed in the following form:

$$\frac{(k_y \cdot h_0)^2}{I} = \frac{f_s \cdot \theta}{2} \Rightarrow \frac{(k_y \cdot h_0)^2}{I} = f(D_{50}, \rho_s, \rho_w, g, u^*) = \text{const.} \tag{20}$$

[62] For the validation of this relation with the channel pattern after 100 years of simulation, the same hierarchical classification of channel order as in the previous section (Figure 7) has been used. For each order of channels, the mean depth of the underlying initial undisturbed bottom is defined as h_0. For the same area of this initial bathymetry the slope I is determined, which is not constant for the different channel orders because the profile has a parabolic shape. From the developed channel pattern, the wave number k_y is established for each order. The average drainage width (W) is defined as the ratio between the length of the ellipse arcs (L_e) connecting the channels of a certain order (Figure 7, right panel) and the corresponding number of channels of the same order (N). Table 3 displays the results. For each order of channels, equation (18) is solved. The resulting values are approximately equal for all orders, which means that the numerical model results are consistent with the theoretical relation.

6. Discussion

[63] In the previous sections a theoretical and a numerical model are presented which are able to describe branching channel systems in a tidal embayment. In this section the results and the model validation are discussed.

[64] The sensitivity computations with the numerical model show that the initial profile influences the channel development. As discussed in section 5, this is considered a timescale issue, because where a pattern has formed, its characteristics are not different from those starting from an equilibrium state. Where no pattern has formed, the underlying profile still has to adapt further to its equilibrium shape, before channels develop. The time needed for this complete morphological process is beyond the present scope of the computation. It should be noted that a static equilibrium state, in the strict sense of zero bed level change everywhere, cannot be obtained with this type of model [see also *Hibma et al.*, 2003b]. The basin profile is considered to be in equilibrium when the morphological changes due to the channel formation are much larger than due to the adaptation of the underlying profile. The initial random perturbations on the bed trigger the pattern formation. Without these perturbations a similar pattern will form, but the time needed for the formation will be larger.

[65] The fact that a well-developed pattern has emerged in the simulation proves that the initial profile is sufficiently close to the equilibrium state for the channel pattern to develop. This supports deriving I and h_0 from this initial bathymetry, instead of the developed pattern, when analyzing the model results.

[66] When checking the validity of the relationship for the field data, a difficulty is encountered in the determination of the underlying equilibrium profile. In this paper, use has been made of the local depth and slope of the channels, but this gives rise to scatter in the results. To verify this approach, the relationship (18) is also evaluated using the local values from the developed channel pattern of the numerical model. The resulting values show slightly more

Table 2. Statistics of the Collected Data From Dutch Wadden Sea

	Friesche Zeegat 57	Friesche Zeegat 87	Vlie	Eierlandse Gat	Born Diep
Depth ratio at bifurcation					
Mean	0.5	0.69	0.53	0.59	0.54
Standard deviation	0.08	0.25	0.06	0.12	0.13
$\frac{h^2}{B^2 I}$					
Mean	0.02	0.17	0.04	0.03	0.02
Standard deviation	0.02	0.14	0.02	0.02	0.02

Table 3. Validation of Equation (18)[a]

Channel Order	h_0	L	I	N	L_e	W	K_y	$\frac{(k_y \cdot h_0)^2}{I}$
1	0.5	389	0.55	37	12500	337.84	0.0186	0.00016
2	1	1095	0.7	20	10900	545.00	0.0115	0.00019
3	3	2737	1.075	6	7800	1300.00	0.0048	0.00020
4	5.5	1340	1.46	2	4000	2000.00	0.0031	0.00020

[a] h_0, mean undisturbed water depth (m); L, mean length of each order of channels (m); I, bottom slope (1/1000); N, number of channels of a certain order; L_e, length of the ellipse arc (m); W, channel drainage width (m); K_y, wave number in lateral direction (m^{-1}).

variation now, but this variation remains sufficiently small to suggest consistency with the relationship.

[67] The validation of the numerical model using Horton's hierarchical analysis showed that Horton's laws are valid for the resulting channel pattern and indicate the branching number of the system. The same approach was applied to field data from the Wadden Sea [*Cleveringa and Oost*, 1999]. They suggest that the channel patterns can be regarded as a dynamic equilibrium configuration because of the similarity in branching between so many investigated systems. It is dynamic, because, despite constant boundary conditions, the system will change continuously. Each tidal channel system oscillates around this equilibrium. At all scales, deviations from the three- or four-times branching network will result in the reestablishment of the stable configuration, either by silting up of superfluous channels, or by the development of new ones.

[68] Considering morphological pattern properties when validating numerical model results is rather unusual. Model simulations are mostly validated by comparing point values. Yet, pattern analysis appears to be a useful addition to the validation process, especially for models simulating general basin morphology instead of an individual inlet.

[69] A last remark on the features formed in the numerical model concerns the ebb-tidal delta. Despite the absence of wind waves, the overall shape of the outer delta looks rather realistic.

[70] While the instability mechanisms leading to self-organization are difficult to extract from the complex numerical model, the theoretical analysis suggests the important parameters straightforwardly. The bed slope, water depth and Shields parameter, which is an indication for the morphological activity, determine the resulting channel pattern. This is in agreement with the controlling parameters for river networks, where the hillslope and threshold-dependent transport phenomena were found to be essential [*Rigon et al.*, 1994]. Furthermore, the theoretical analysis shows that curvature-induced secondary flow has no influence on the dominant wave number and therefore does not have to be taken into account for the reproduction of branching channel structures using a numerical model. The negligible influence of secondary flow in the feedback mechanisms leading to channel shoal formation in elongated basins was also found by *Coeveld et al.* [2003; also see *Hibma et al.*, 2004].

7. Conclusion

[71] The theoretical analysis and the Delft3D numerical model both reliably predict key properties of branching channel patterns in tidal basins. Hence they provide new tools to study tidal channel networks. The theoretical analysis shows that the branching channel pattern in a tidal basin is governed by the morphological properties (represented by the overall bottom slope and the water depth), the tidal flow strength and the sediment properties (together represented by the Shields parameter). A relation between the number of channels per unit span and these physical parameters of the basin is found. The relation shows smaller and more closely spaced channels for larger overall bottom slopes, for a morphologically more active system (larger Shields parameter) and for smaller water depths. Quantitatively it implies that the water depth should halve at every bifurcation. All these features agree well with field observations and the results of the numerical model.

[72] If the initial basin hypsometry is not too far from equilibrium, the numerical model produces a well-developed channel pattern. The resulting channel network displays a three-times branching behavior that is similar to the three- to four-times branching patterns observed in the Wadden Sea basins. Moreover, we argue that the numerical and the analytical models agree well with each other. The pattern analysis presented herein provides for another validation test for numerical models of this type of phenomena, in addition to the conventional point-by-point comparison of model results with data.

[73] **Acknowledgments.** The work presented herein was done in the framework of CORILA (Consorzio per la gestione del centro di Coordinamento delle attivitá di Ricierca inerenti il Sistema Lagunare di Venezia) and the DIOC program "Hydraulic Engineering and Geohydrology" of Delft University of Technology, Theme 1, Project 1.4. It is embedded as such in Project 03.01.03 (Coasts) of the Delft Cluster strategic research program on the sustainable development of low-lying deltaic areas. The first author gratefully acknowledges the Socrates-Erasmus program for enabling him to spend 6 months in Delft to work on this subject. WL/Delft Hydraulics is acknowledged for providing access to the Delft3D software package.

References

Allen, J. R. L. (2000), Morphodynamics of Holocene salt marshes: A review sketch from the Atlantic and southern North Sea coasts of Europe, *Quat. Sci. Rev.*, *19*(17–18), 1155–1231.

Biegel, E. J. (1991), Equlibrium relations in the ebb tidal delta, inlet and bachbarrier area of the Frisian inlet system, *Rep. GEOPRO 1991.028/GWAO-91.016*, Univ. of Utrecht, Netherlands.

Biegel, E. J. (1993), Morphological changes due to sea level rise in tidal basins in the Dutch Wadden Sea versus concepts morphological response model MORRES, report, Inst. for Mar. and Atmos. Res. Utrecht Univ. of Utrecht, Netherlands.

Cleveringa, J., and A. P. Oost (1999), The fractal geometry of tidal-channel systems in the Dutch Wadden Sea, *Geol. en Mijnbouw*, *78*, 21–30.

Coeveld, E. M., A. Hibma, and M. J. F. Stive (2003), Feedback mechanisms in channel-shoal formation, paper presented at the Coastal Sediments Conference, St. Petersburg, Fla., 18–23 May.

De Vriend, H. J. (1996), Mathematical modeling of meso-tidal barrier island coast. Part I: Empirical and semi empirical model, in *Advances in Coastal and Ocean Engineering*, edited by P. L.-F. Liu, pp. 115–149, World Sci., River Edge, N. J.

De Vriend, H. J., and J. S. Ribberink (1996), Mathematical modeling of meso-tidal barrier island coast. Part II: Process-based simulation model, in *Advances in Coastal and Ocean Engineering*, edited by P. L.-F. Liu, pp. 151–197, World Sci., River Edge, N. J.

Engelund, F., and E. Hansen (1967), *A Monograph on Sediment Transport in Alluvial Streams*, 62 pp., Teknisk Forlag, Copenhagen.

Fagherazzi, S., and D. J. Furbish (2001), On the shape and widening of salt marsh creeks, *J. Geophys. Res.*, *106*, 991–1003.

Fagherazzi, S., A. Bortoluzzi, W. E. Dietrich, A. Adami, M. Marani, S. Lanzoni, and A. Rinaldo (1999), Tidal networks: 1. Automatic network extraction and preliminary scaling features from digital terrain maps, *Water Resour. Res.*, *35*, 3891–3904.

Fokkink, R. (1993), Fundamental considerations on morphodynamic modeling in tidal regions, *Rep. Z331*, Delft Hydraul., Delft, Netherlands.

Friedrichs, C. T., and D. G. Aubrey (1996), Uniform bottom shear stress and equilibrium hypsometry of inter-tidal flats, in *Mixing in Estuaries and Coastal Seas*, *Coastal Estuarine Ser.*, vol. 50, edited by C. Pattiaratchi, pp. 405–429, AGU, Washington, D. C.

Friedrichs, C. T., and J. E. Perry (2001), Tidal salt marsh morphodynamics, *J. Coastal Res.*, *27*, 7–37.

Hayes, M. O. (1975), Morphology of sand accumulation in estuaries: An introduction to the symposium, in *Estuarine Research II*, edited by L. E. Cronin, pp. 3–22, Academic, San Diego, Calif.

Hibma, A., H. J. De Vriend, and M. J. F. Stive (2003a), Numerical modeling of shoal pattern formation in well-mixed elongated estuaries, *Estuarine Coastal Shelf Sci.*, *57*, 981–991.

Hibma, A., H. M. Schuttelaars, and Z. B. Wang (2003b), Comparison of longitudinal equilibrium profiles of estuaries in idealized and process-based models, *Ocean Dyn.*, *53*, 252–269.

Hibma, A., M. J. F. Stive, and Z. B. Wang (2004), Estuarine morphodynamics, *Coastal Eng.*, *51*, 765–778.

Horton, R. E. (1945), Erosional development of streams and their drainage basins: Hydrophysical approach to quantative morphology, *Geol. Soc. Am. Bull.*, *56*, 275–370.

Jeuken, M. C. J. L. (2000), On the morphologic behavior of tidal channels in the Westerschelde estuary, Ph.D. thesis, 378 pp., Univ. of Utrecht, Netherlands.

Kirchner, J. W. (1993), Statistical inevitability of Horton's laws and the apparent randomness of stream channel networks, *Geology*, *21*, 591–599.

Lanzoni, S., and G. Seminara (2002), Long-term evolution and morphodynamic equilibrium of tidal channels, *J. Geophys. Res.*, *107*(C1), 3001, doi:10.1029/2000JC000468.

Marani, M., E. Belluco, A. D'Alpaos, A. Defina, S. Lanzoni, and A. Rinaldo (2003), On the drainage density of tidal networks, *Water Resour. Res.*, *39*(2), 1040, doi:10.1029/2001WR001051.

O'Brien, M. P. (1969), Equilibrium flow areas of inlets on sandy coasts, *J. Waterw. Harbour Div. Am. Soc. Civ. Eng.*, *95*, 43–52.

Officer, C. B. (1976), *Physical Oceanography of Estuaries (and Associated Coastal Waters)*, John Wiley, Hoboken, N. J.

Oost, A. P. (1995), Dynamics and sedimentary development of the Dutch Wadden Sea with emphasis on the Frisian inlet, report, Inst. voor Aardwetenschappen Rijksuniv., Utrecht, Netherlands.

Pritchard, D., A. J. Hogg, and W. Roberts (2002), Morphological modeling of inter-tidal mudflats: The role of cross-shore tidal currents, *Cont. Shelf Res.*, *22*, 1887–1895.

Rigon, R., A. Rinaldo, and I. Rodriguez-Iturbe (1994), On landscape self-organization, *J. Geophys. Res.*, *99*, 11,971–11,993.

Rinaldo, A., S. Fagherazzi, S. Lanzoni, M. Marani, and W. E. Dietrich (1999a), Tidal networks: 2. Watershed delineation and comparative network morphology, *Water Resour. Res.*, *35*, 3905–3917.

Rinaldo, A., S. Fagherazzi, S. Lanzoni, M. Marani, and W. E. Dietrich (1999b), Tidal networks: 3. Landscape-forming discharges and studies in empirical geomorphic relationships, *Water Resour. Res.*, *35*, 3919–3929.

Rodriguez-Iturbe, I., M. Marani, R. Rigon, and A. Rinaldo (1994), Self-organized river basin landscapes: Fractal and multifractals characteristics, *Water Resour. Res.*, *30*, 3531–3539.

Roelvink, J. A., and G. K. F. M. van Banning (1994), Design and development of DELFT3D and application to coastal morphodynamics, in *Hydroinformatics*, edited by A. Verwey et al., pp. 451–456, A. A. Balkema, Brookfield, Vt.

Schuttelaars, H. M. (2000), One-dimensional long-term equilibra in tidal embayments, in *Interactions Between Estuaries, Coastal Seas and Shelf Seas*, edited by T. Yanagi, pp. 125–137, Terra Sci., Tokyo.

Schuttelaars, H. M., and H. E. de Swart (1996), An idealized long-term morphodynamic model of a tidal embayment, *Eur. J. Mech. B Fluids*, *15*, 55–80.

Stelling, G. S. (1984), On the construction of computational methods for shallow water flow problems, *Rijkswaterstaat Comm.*, *35*, 224 pp.

Stive, M. J. F., and Z. B. Wang (2003), Morphodynamic modeling of tidal basins and coastal inlets, in *Advances in Coastal Modeling*, edited by C. Lakhan, chap. 13, pp. 367–392, Elsevier Sci., New York.

Struiksma, N., K. W. Olesen, C. Flokstra, and H. J. De Vriend (1985), Bed deformation in curved alluvial channels, *J. Hydraul. Res.*, *23*, 57–79.

van Veen, J. (1950), *Ebb and Flood-Channel Systems in the Netherlands Tidal Waters* (in Dutch with English summary), *KNAG 2e Ser.*, part 67, Delft Univ. of Technol., Netherlands.

Wang, Z. B. (1992), Fundamental considerations on morphodynamic modeling in tidal regions, *Rep. Z331*, part I, Delft Hydraul., Delft, Netherlands.

Wang, Z. B., H. J. De Vriend, and T. Louters (1991), A morphodynamic model for a tidal inlet, in *Computer Modeling in Ocean Engineering 91*, edited by A. S. Arcilla et al., pp. 235–245, A. A. Balkema, Brookfield, Vt.

Wang, Z. B., T. Louters, and H. J. de Vriend (1995), Morphodynamic modeling of a tidal inlet in the Wadden Sea, *J. Mar. Geol.*, *126*, 289–300.

A. Defina, Dipartimento Ingegneria Idraulica Marittima Ambientale e Geotecnica, Universitá di Padova, I-35122, Padova, Italy. (defina@idra.unipd.it)

A. Hibma, R. Marciano, H. J. de Vriend, and Z. B. Wang, Delft University of Technology, P.O. Box 5048, 2600 GA, Delft, The Netherlands. (ahi@vanoord.com; raffaele.marciano@inwind.it; huib.devriend@wldelft.nl; zheng.wang@wldelft.nl)